International Symposium
On Turbulence and Shear Flow
Phenomena (TSFP-8)
August 28 - 30, 2013 Poitiers, France

FLUKEPRINTS OF CETACEANS AND THE CORRESPONDING SHEAR FLOW PHENOMENON

Germain Rousseaux
Pprime Institute, UPR 3346,
CNRS - Université de Poitiers - ISAE ENSMA,
11 Boulevard Marie et Pierre Curie,
Téléport 2, BP 30179,
86962 Futuroscope Cedex, France.
germain.rousseaux@univ-poitiers.fr

David Uminsky
Department of Mathematics,
University of San Francisco,
2130 Fulton Street,
San Francisco, CA 94117-1080, USA.
duminsky@usfca.edu

Rachel Levy
Harvey Mudd College
301 Platt Blvd, Claremont, CA 91711, USA.
levy@g.hmc.edu

ABSTRACT

When walking in the snow, mud or sand, our feet leave a characteristic imprint in the medium. The naturalists, hunters or paleontologists use them to identify animals. The medium have plastic properties which allow the persistence of the footprint. Here, we consider another kind of footprint, in a fluid medium, whose essential property is its ephemeral nature much like wake vortices after the take-off of an aircraft. We study the flukeprint of cetaceans at the surface of water. We will present laboratory experiments with an artificial fluke which show that the formation of flukeprints is mainly a wave-current interaction process with a peculiar shear flow.

INTRODUCTION

Free propagation of waves is an exception. For example, in a marine environment, water waves are refracted by the varying landscape of the ocean floor as they approach the seashore and ocean currents modify wave propagation (Mei et al., 2005). The landscape of waves on the ocean surface is complex, with interactions of both gravity and capillary waves with currents. We consider wave interactions that have fascinated both casual whale-watchers and marine biologists: cetacean flukeprints made by whales (Fig. 1), dolphins (Fig. 2) or porpoises. In the ocean, these patterns are sometimes known as "whale footprints". A cruising or diving whale generates in its wake a series of oval-shaped patches of water with a smoother interface compared to the surrounding roughness of the sea surface (Fig. 1). According to Ken Brower from National Geographic (Brower, 2010), *"When a whale or dolphin swims at shallow depths, turbulence from its flukes rises to form a circular slick on the surface: the footprint or flukeprint. The flukeprints of blue whales are large and surprisingly persistent. The smooth patch lingers long after the whale is gone. "It's a measure of how much energy is in the stroke," Mate told me one afternoon when he caught me staring at one of these slicks. The circle of the flukeprint is perfectly smooth, except for a few faint curves that mark the continued upwelling of energy. Eventually the chop of the ocean begins to erode the slick from the outside inward, but only slowly"*.

Figure 1. Flukeprint created in the open ocean by a fin whale.

These surface signatures are characterized by a smooth oval pattern where short gravity waves cannot penetrate. Depending on flow conditions, one may also observe several radii surrounding the smooth oval corresponding to mode conversion into blue-shifted and capillary waves. In this paper we will show that the key explanation of flukeprint formation, involves the dispersive properties of water waves along with the effect of gravity, as well as surface tension and wave-breaking in the mode conversion induced by the surface currents. Similar surface patterns occur when a vortex ring created by an upward-pointing jet interacts with a free surface, although these patterns are simpler due to the regular shape of the jet orifice. Another re-

lated example is a circular hydraulic jump in which a jet of water impacts a solid plate and creates a disk-shaped region with a boundary that surface waves cannot penetrate (Jannes et al., 2011). Long shallow water waves are blocked by the flow induced on the plate by the impacting jet with a characteristic border, namely the jump. In essence, the flukeprint is an inverted circular jump caused by a jet-like flow induced by a vortex ring obliquely impacting the ocean surface with different dispersive properties.

We begin by discussing the physical mechanisms leading to the formation of flukeprints. Then, we provide PIV measurements from experiments reported by us in (Levy et al., 2011) where an oscillating 2D polypropylene fluke created vortex rings and resulting surface prints were visualized by particles and a laser sheet.

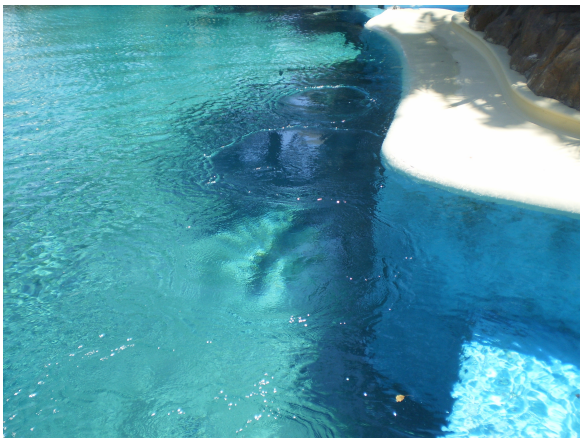

Figure 2. A sequence of four flukeprints created by a dolphin in a swimming pool. The flukeprints grow in size over time, so the small prints are the ones made most recently by the dolphin traveling from "bottom to top" (dolphin fluke is visible at the top of the picture).

FLUKEPRINT FORMATION THROUGH WAVE-CURRENT INTERACTION

Our goal is to model the wave interactions in the flukeprint phenomenon using existing theory of wave-current interaction. Since the ocean is deep, we consider the deep water limit. The current induced by the whale will be modeled with a uniform velocity U throughout the depth, which is a simplification of the flow in a flukeprint. In practice, we hypothesize that the wavelength is shorter than the vertical distance in which the flow is sufficiently plug-like and strong enough to stop the waves. In deep water and without surface tension, when a gravity wave meets a counter-current, the incident wavelength diminishes (the phenomenon known as blue-shifting) because of normal dispersion. That is, the wave group velocity c_g is a decreasing function of the wavenumber k. In this regime, the blocking of pure gravity waves is then described by the following formula (Nardin et al., 2009):

$$U_g = -\frac{gT}{8\pi} \qquad (1)$$

where g is the gravity. This equation indicates that the blocking velocity is linearly related to the wave period T. We expect wave blocking if the period of the existing gravity waves is short, but no blocking if the period is long. *This simple formula explains the presence of only long waves inside the flukeprints and has not previously been noted.* Since the blocking velocity in deep water depends on the wave period, it is an intrinsically dispersive effect whereas in shallow water the blocking occurs for a velocity which depends only on the water depth h that is $U_h = -\sqrt{gh}$ (Peregrine, 1976 ; Dingemans, 1997).

Moreover, the wave amplitude A increases because of the conservation of the density of wave action flux (Peregrine, 1976):

$$\frac{Ec_g}{\omega - Uk} = constant \qquad (2)$$

where $E = 1/2\rho g A^2$ is the wave energy averaged on a period with a fluid density ρ. According to the WKBJ approximation, in which the scale of flow variation is longer than the wavelength, the wave amplitude would diverge during blocking since the group velocity c_g of the system (wave + current) tends to zero. Hence, the energy of water waves increases indefinitely since it scales with the square of their amplitude. However, this caustic for the energy can be avoided by several regularization processes for the amplitude: one linear and the other nonlinear. In the linear amplitude case, the incoming waves are diffracted by the current and blue-shifted waves appear by mode conversion. Part of the energy of the incoming waves is reflected into blue-shifted waves since their group velocity is negative; wave blocking can then occur because the wavefront folds on itself. Since both waves have the same wave-number at the blocking location, they interfere. The interference pattern is not a simple standing wave which results from the superposition of the same reflected wave but is modified by the diffraction due to the current. If the amplitude of the incident wave stays small, we should observe an Airy like-pattern at the boundary of the flukeprint, similarly to the principal arc and supernumerary arcs of a rainbow (Nardin et al., 2009). In the non-linear amplitude case, wave breaking occurs because of the amplification of the wave amplitude. The Airy pattern is either strongly modified by nonlinearity or disappears because of wave breaking. If the maximum of the Airy wave envelope reaches a wave breaking criterion such that the wave steepness $k \times A$ reaches a threshold value, then physical effects can result like foaming or turbulence seen at the boundary of whale flukeprints as observed by whale watchers and marine biologists, see Fig. 1 of (Levy et al., 2011). When including surface tension, Badulin et al. (Badulin, 1983) observed that as long as the counter-current is strong enough, gravity waves can still be blocked in deep waters. In addition, blue-shifted waves appear by mode conversion as in the pure gravity case but are also stopped while drifting backward at a new blocking boundary, formed where the blue-shifted wave merges with a new capillary solution (Badulin, 1983; Trulsen and Mei, 1993; Rousseaux et al., 2010). Capillary waves appear at this secondary blocking frontier, described in (Rousseaux et al., 2010), and propagate in the same direction as the incident gravity waves, provided the regime stays linear. Ultimately, the capillary waves no longer propagate far inside the flukeprint because they are not only quickly damped by viscosity but they are no longer solutions of the dispersion

relation (Rousseaux et al., 2010), and are seen on its boundary. The threshold velocity for the appearance of capillary waves in deep water on a plug-like flow current is $U_\gamma - 2\pi\frac{l_c}{T}$ where $U_\gamma = \sqrt{2}\left(\frac{\gamma g}{\rho}\right)^{1/4}$ is the minimum of the phase velocity as a function of the wavenumber and where $l_c = \sqrt{\frac{\gamma}{\rho g}}$ is the capillary length (Rousseaux et al., 2010). The previous discussion is valid provided the water is sufficiently deep and the vertical flow is plug-like. However, experiments reveal a more complicated picture not currently handled by the theory.

In addition to its influence on the mode conversion, surface tension can play another role in the flukeprint formation since it also changes because of variation in surfactant concentration or temperature. This phenomenon in which surface tension is non-increasing as the temperature or surfactant concentration increases is referred to generically as a Marangoni effect. Oily skin sloughed by cetaceans may also modify the properties of the air-water interface, but in a different way than just changing the value of surface tension. An oil monolayer can feature a surfactant concentration gradient (Gibbs-Marangoni effect) because of the motion of water waves (Behroozi, 2007). This induces a surface dilatational elasticity (Gibbs surface elasticity) related to the presence of elastic longitudinal waves within the monolayer. The resulting rigidity of the surface dampens the capillary waves (which constitutes the Franklin effect) by increasing the shear forces on the free surface hence the viscous dissipation. Moreover, capillary waves are naturally dampened by viscosity and their amplitude is known to decreases exponentially with a factor proportional to the water viscosity μ and inversely proportional to surface tension γ and wave period T: $A = A_0 e^{-\frac{2\pi\mu}{T\gamma}}$ (Behroozi, 2007). Hence, a decrease of surface tension quickly dampens capillary waves. In addition to the blocking of short gravity waves by the induced flow created by the vortex ring, the Franklin effect may provide another mechanism for the damping of capillary waves in addition to their usual dissipation by viscosity.

Recently, it was demonstrated (Churnside, 2009) using thermal imagery that the inside of flukeprint has a colder water temperature than the outside. This temperature signature is a natural consequence of the vortex ring inducing a jet of water taking cold water from below the free surface and dispatching it at the surface forming the interior of the flukeprint. The thermal signature provides one way to track whales. However, it must be noted that the thermal change is not the origin of the print. A decrease in temperature will increase the surface tension, hence decrease the viscous damping of the capillary waves.

A MOCK WHALE IN THE LABORATORY

To visualize vortex ring formation and the resulting surface patterns, Levy et al. (2011) conducted a series of experiments in collaboration with Flo-Metrics in San Diego using a tank of water approximately 122 cm long by 61 cm wide by 49 cm deep (Fig. 3). A 2D fluke shape made of slightly flexible polypropylene (0.16 cm thick) with the boundary shape scaled up from a photograph of a blue whale fluke was oscillated in the water. The mock fluke was 0.2 m tip to tip, whereas blue whale flukes are typically 5-6 m.

We computed the velocity field using particle image velocimetry (PIV) on images of a laser sheet and small particles similar to Kaleiroscope. The laser sheet illuminating the small flakes was created using a 1 Watt green laser directed through a 3 mm diameter stirring rod.

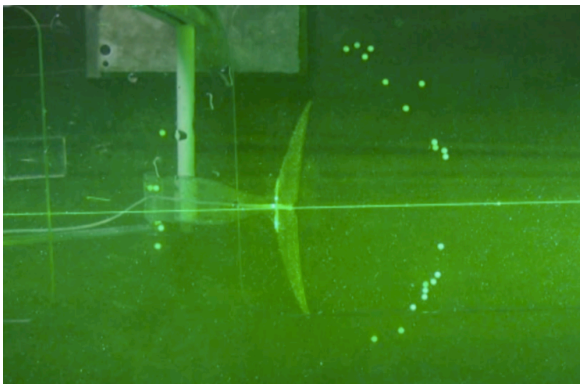

Figure 3. Experimental setup and top view of the artificial fluke with white tracers on the free surface.

The PIV gives crucial information on the velocity field needed in the theory to derive the dispersion relation used to compute the blocking boundary of the flukeprint. Here, there are no waves in the experiments since we deliberately focus on the modification of the dispersion relation induced by the peculiar flow profile generated by the whale compared to the usual plug-flow assumption (no vorticity) when dealing with wave-current interaction and which neglects vertical variations of the velocity. In each experimental run, oscillations were maintained at 0.32 Hz and there was no forward motion. For comparison, blue whale fluke oscillations occur at about 0.5-1.0 Hz with forward velocity 1-1.5 m/s. The initial angle of the fluke with the plane of the surface was varied, and we recorded videos at 30 fps. Stills from these videos were first reported in (Levy et al., 2011) but did not include PIV. Here, PIV measurements from several runs initiated at 12.5 and 60 degrees from horizontal are reported. Each trial consisted of one oscillation from the prescribed angle, down 25 degrees and then up. The image processing is completed on a personal computer with the software Davis 7.2 from Lavision. Coordinate x denotes the cruise direction of the whale, y the transverse direction and z the vertical direction.

THE FLOW INDUCED BY A MOCK WHALE

According to Archer et al. (2010), the life-time of a vortex ring interacting with a free surface at 90° of incidence features three stages after creation: approach of the free surface, slowing and expansion. The PIV measurements show that an outgoing flow is induced on the surface of water from the center of a patch with an oval shape, see Fig. 4. The induced surface current is anisotropic and time-dependent; it is stronger on the rear of the flukeprint than on the front. Our Fig. 4 (top) is very similar to the numerical simulations reported in (Lugt and Ohring, 1994; Ohring and Lugt, 1996) where a vortex ring impacts obliquely a free surface. On average, the flow is weaker in the center of the flukeprint than on its boundary. The streamlines (not reported here) features a null-line from which all streamlines radiate outward. The strikelines (perpendicular to the streamlines) display a typical oval shape reminiscent of field observations, see Fig. 4 (bottom).

In Fig. 5 (top) a quadrupole is seen behind the mock fluke. The quadrupole corresponds to the successive emis-

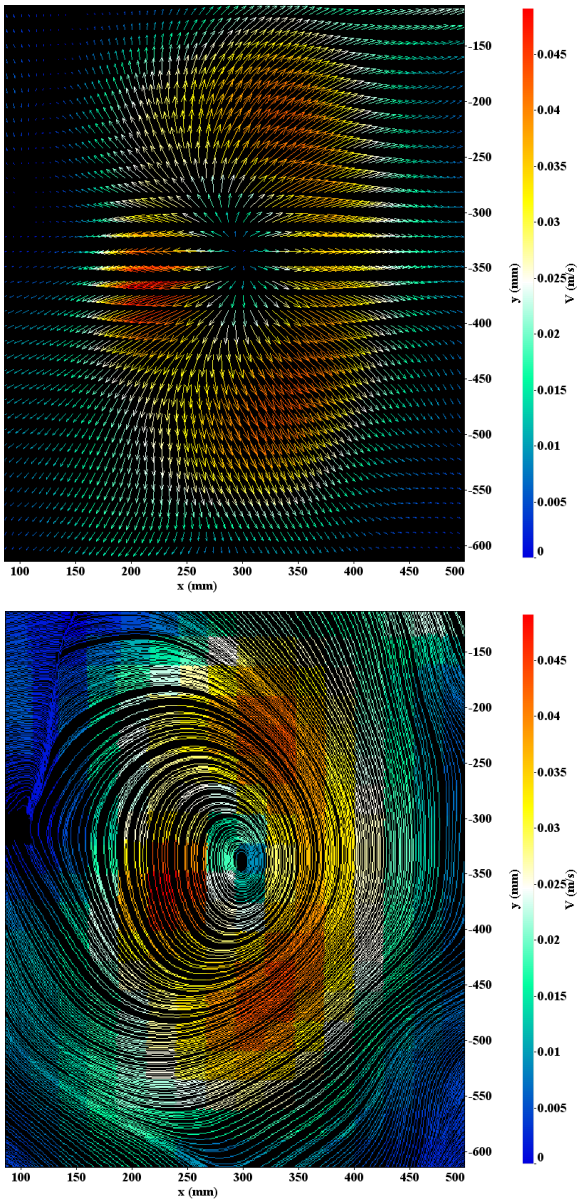

Figure 4. Surface flows. Top: Typical instantaneous velocity field on the free surface created by an impacting vortex ring (t=0.266s after flapping begins). The fluke is oriented as if the whale is facing left and the flow is stronger on average on the right. The colors correspond to the modulus of the velocity at each point. The angle of the fluke at the maximum is 60° and it oscillates through a 25° arc. Bottom: Corresponding strikelines (perpendicular to the streamlines of the flow) which display an oval-shape flow print similar to the surface flukeprint as seen by the observers. The colors correspond to the modulus of the velocity at each point.

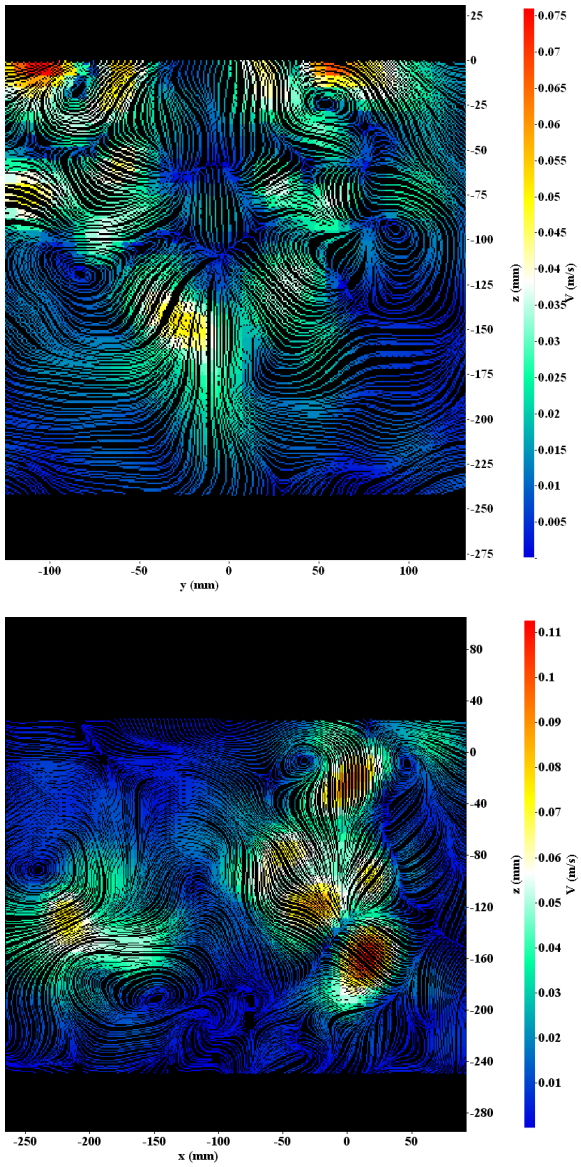

Figure 5. Vortex rings. Top: Back view of the whale (t=4.2s after flapping begins). Typical quadrupolar flow on the rear of the fluke. Cross-sections of the two vortex rings. The angle of the fluke is 60°. Bottom: Side view (t=3.6s after flapping begins). Streamlines of the flow. One observes the cross-section of the two vortex rings created during the downward and the upward motions of the fluke. The upper ring creates free surface shear flows which will block the waves. The colors correspond to the modulus of the velocity at each point. The angle of the fluke is 60°.

sions of two vortex rings observed from the side: one towards the deep in the downward motion of the fluke, one towards the free surface in the upward motion of the fluke, see Fig. 5 (bottom). Measurements of the surface flow profile in the radial direction demonstrate the inhomogeneity of the flow as one gets far from the center ($y = 0$) of the flukeprint, see Fig. 6. The radial velocity increases almost linearly with the distance to center before reaching a maximum and then decreases to zero. The radial flow depends on the vertical position as seen on the Fig. 6 (bottom). In these experiments, the PIV indicates that the flow is almost linear with the depth with a flow reversal below the core of the toroidal vortex tube.

An enormous challenge for the theoretical work will be to derive a dispersion relation with a changing vertical and horizontal vorticity as exemplified in the Figures 6 and 7. Recently but with the constraint that the relationship between the vorticity and stream function is known, Karageorgis derived the implicit dispersion relation for the velocity profile of any non-constant vorticity (Karageorgis, 2012).

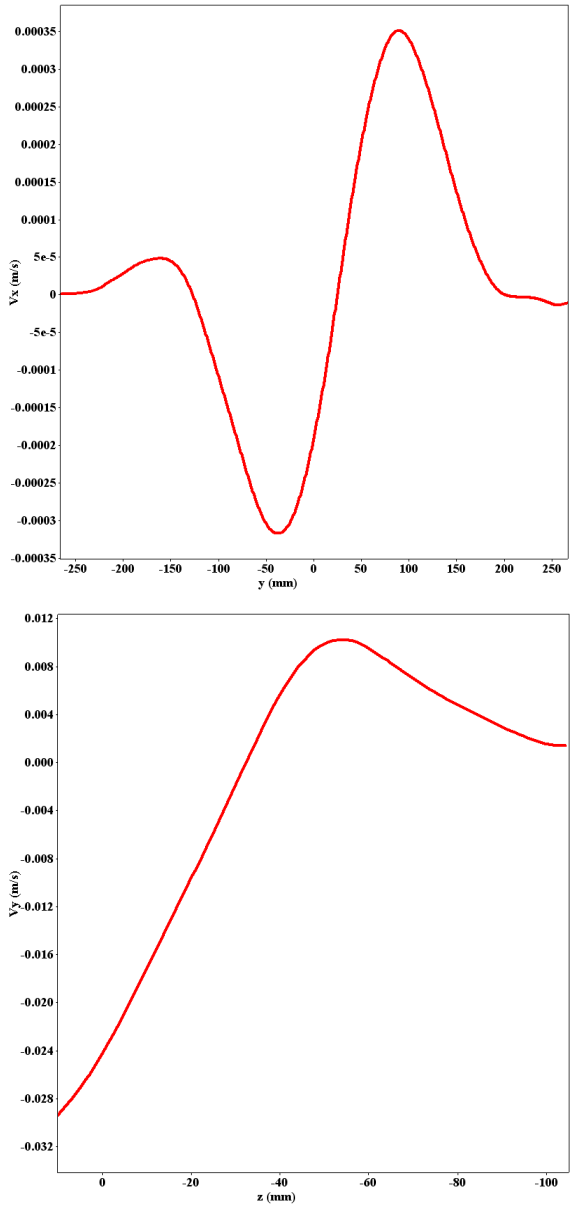

Figure 6. Velocity profiles. Top: Back view of the whale (z=-10mm below the free surface). Typical longitudinal variation of the radial surface flow induced by the upper vortex ring (t=2.6s after flapping). Bottom: Back view of the whale (x=-132mm on the left of the upper vortex ring center). Typical vertical variation of the radial surface flow induced by the upper vortex ring (t=8.4s after flapping). Starting at an initial 12.5° from the surface, the fluke oscillates through an arc of ±25°.

CONCLUSIONS AND PERSPECTIVES

To conclude, the existing theory for wave-current interactions includes a number of simplifying assumptions. The first, of course, is that we assume the flow is in one or two dimensions rather than providing a fully 3D model. Even in the 2D case, our measurements show that the surface flow generated in the whale flukeprint is anisotropic in the radial direction. Another simplification is the assumption that the flow has usually a uniform velocity profile on the entire depth, or on a given depth (Taylor, 1955) or at most a linear velocity profile on the entire depth (Thompson, 1949; Biesel, 1950; Burns, 1953; Tsao, 1957; Fenton, 1973; Brevik, 1976; Kirby and Chen, 1989; Kantarzhi, 1898; Nepf, 1994) or on given depth (Taylor, 1955). The PIV displays a flow reversal in the vertical direction in addition to a maximum in the radial direction. The current approach to treat complicated velocity profiles is to modify the dispersion relation using a depth-averaged flow (Skop, 1987; Kirby and Chen, 1989) but there is no consensus that this result is correctly capturing the physics. Some of the most promising numerical work in this direction is the research of Archer et al. (2010) who has computed solutions for flows containing a vortex ring interacting with a free surface: here time dependence can also be taken into account. The extreme difficulty in describing flukeprint formation by applying our knowledge of wave-current interaction is that we do not have the dispersion relation for the flow induced by the whale. One exception is the work of Skop (1987), which considers a simple jet-like flow and assumes a triangular velocity profile in the vertical direction. This jet-like flow could treat the first stage of the flukeprint formation when the vortex ring approaches the free surface. Then, the dispersion relation taking into account a flow reversal during the vortex ring expansion has to be derived theoretically in the spirit of Karageorgis (Karageorgis, 2012) and then solved. WKB theory cannot be applied at the current stage since one must known the dispersion relation in order to compute the rays and blocking.

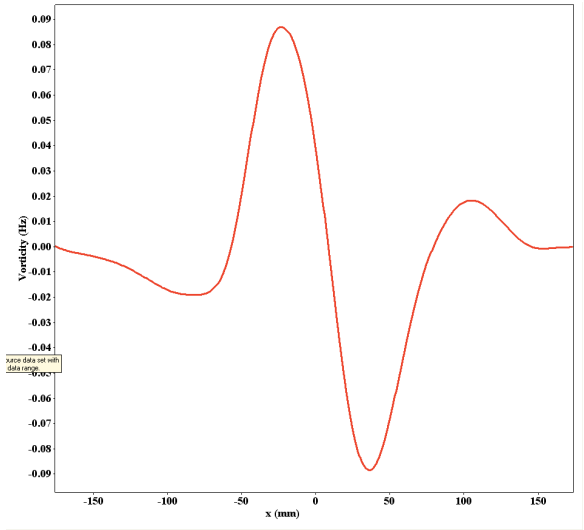

Figure 7. Vorticity as a function of the distance to the flukeprint center ($x = 0$ here) for a depth $z = -15$ mm. The angle of the fluke is 60°.

ACKNOWLEDGMENTS

The authors thank David Lee and Justin Holmes for providing the beautiful pictures of the dolphin flukeprints.

REFERENCES

C. C. Mei, M. Stiassnie and D. K. P. Yue *Theory and Applications of Ocean Surface Waves* (World Scientific, 2005).

G. Jannes, R. Piquet, P. Maïssa, C. Mathis and G. Rousseaux, Physical Review E, **83** (5), 056312 (2011).

K. Brower, Blue Whales, National Geographics, March 2009.

R. Levy, D. Uminsky, A. Park and J. Calambokidis, Int. J. Nonlin. Mech., **46** (4), 616-626 (2011).

J.-C. Nardin, G. Rousseaux and P. Coullet, Physics. Phys. Rev. Lett., **102** (12), 124504-1/4 (2009).

D. H. Peregrine, Adv. Appl. Mech., **16**, 9-117 (1976).

M. W. Dingemans *Water Wave Propagation over Uneven Bottoms* (World Scientific, 1997).

S. I. Badulin, K. V. Pokazeev and A.D. Rozenberg, lzv. AN. SSSR, FAO, **19** (10), 1035-1041 (1983).

K. Trulsen & C. C. Mei, J. Fluid Mech., **251**, 239-271 (1993).

G. Rousseaux, P. Maïssa, C. Mathis, P. Coullet, T. G. Philbin and U. Leonhardt, New J. Phys., **12**, 095018 (2010).

J. Churnside, L. Ostrovsky and T. Veenstra, Oceanography, **22**, 206-209 (2009).

P. Behroozi, K. Cordray, W. Griffin and F. Behroozi, Am. J. Phys., **75** (5), 407-414 (2007).

P. J. Archer, T. G. Thomas and G. N. Coleman, J. Fluid Mech., **642**, 79-94 (2010).

H. Lugt and S. Ohring, Meccanica, **29**, 313-329 (1994).

S. Ohring and H. Lugt, Meccanica, **31**, 623-655 (1996).

P. Karageorgis, Eur. J. Mech. B Fluids, 34, 712 (2012).

G. I. Taylor, Proc. R. Soc. Lond. A, 231, 466-478 (1955).

P. D. Thompson, Ann. N.Y. Acad. Sci., **5**, p. 463-474 (1949).

F. Biesel, La Houille Blanche, **5**, p. 279-285 (1950).

J. C. Burns, Proc. Camb. Phil. Soc., **49**, p. 695-705 (1953).

S. Tsao, J. Geophys. Res., **79**, p. 4498-4508 (1957).

J. D. Fenton, J. Inst. Math. Appl., **12**, p. 1-20 (1973).

I. Brevik, Phys. Norvegica, **8**, p. 157-162 (1976).

J. T. Kirby and T. M. Chen, J. Geophys. Res., **94**, 10131027 (1989).

I. G. Kantarzhi, I. L. Makarova and YE. N. Pelinovskiy, Oceanology, Vol. 29, No. 2, 145-150 (1989).

H. M. Nepf & S. G. Monismith, Appl. Ocean. Res., **16** (5), 313-315 (1994).

R. A. Skop, J. Waterw., Port, Coastal, Ocean Eng., **113**, 187-195 (1987).